City, University of London Institutional Repository

This is the accepted version of the paper.

This version of the publication may differ from the final published version.

Compact and Fabrication-tolerant Polarization Splitter Based on Horizontal Triple-slot Waveguide

Weifeng Jiang,[1,2,*], Xiaohan Sun[1], and B. M. Azizur Rahman[2]

[1]*National Research Center for Optical Sensing/Communications Integrated Networking, Department of Electronics Engineering, Southeast University, Nanjing 210096, China*
[2]*Department of Electrical and Electronic Engineering, City, University of London, Northampton Square, London EC1V OHB, UK*
Corresponding author: jwf@seu.edu.cn

A compact and fabrication-tolerant polarization beam splitter (PBS) based on the horizontal triple-slot waveguides is proposed and optimized by using the rigorous H-field based full-vectorial finite element method (VFEM) and the least squares boundary residual (LSBR) method. It can be noted from the simulation results that a fabrication-tolerant PBS with a compact length of 33 μm can be yielded based on the horizontal triple-slot waveguides. The polarization extinction ratios (PERs) are -21.8 dB and -20.3 dB at 1.55 μm wavelength for the quasi-TE and quasi-TM modes, respectively. The 1 dB bandwidth is 100 nm for both the polarizations. The fabrication tolerances are also thoroughly calculated for the proposed PBS. © 2016 Optical Society of America

1. Introduction

Silicon photonics is a promising technique for building the high-density photonic integrated circuits (PICs) [1,2]. Using highly sophisticated complementary-metal-oxide-semiconductor (CMOS) compatible process, silicon photonics can offer a low-cost PIC platform with a small footprint due to a very high index-contrast. However, a silicon waveguide is naturally polarization dependent due to the structural birefringence [3,4]. To circumvent this issue, a polarization beam splitter (PBS) and rotator are generally utilized to build a polarization-independent circuit [5,6]. A PBS is of considerable importance in the polarization-diversity system, which aims to split two orthogonal quasi-transverse-electric (TE) and quasi-transverse-magnetic (TM) polarizations into two individual channels, respectively.

Many approaches, including various design approaches and materials, have been reported to build a PBS [7-11]. One approach could be the use of a hybrid plasmonic waveguide (HPW), which has been extensively studied and can yield an ultra-compact broadband PBS [12]. Nevertheless, a HPW suffers from the inherent metallic absorption and complicated fabrication process. Another approach could be the use of the directional couplers (DCs), including the symmetrical and asymmetrical DCs [13,14]. Although a symmetrical DC can achieve a simple and easy-design PBS, but it usually suffers from a long length, as a result of the weak birefringence [15]. Instead, a compact PBS with a length of less than 10 μm can be obtained by using an asymmetrical DC (ADC) [16]. However, either the loading refractive index/waveguide or non-trivial fabrication technique is needed for the ADC based PBS. In addition, the ADC based PBS suffers from the tight fabrication tolerance. Another approach could be the use of a multimode interference (MMI)-based PBS, which can yield a high extinction ratio (ER) of more than 22 dB [17]. Nevertheless, an MMI-based PBS is always with an exceedingly long length, though that can be trimmed by utilizing a quasi-state imaging effect. Another approach could be the use of a grating-assisted coupler, which can achieve a compact PBS and a moderate working bandwidth (~40 nm) [18]. But, this approach requires a quite complex design and relatively difficult fabrication process.

Recently, slot waveguides are showing great promise for developing high performance and compact photonic devices [19-21]. The normal electric field of the slot waveguide enhances due to a big discontinuity from a very high index-contrast between the low-index slot and the high-index layers. Therefore, the optical field can be confined and guided in the low-index slot region. The slot waveguides can be divided into the vertical-slot and horizontal-slot waveguides for the quasi-TE and quasi-TM modes confinement, respectively. Owing to their strong polarization-dependence, several PBSs have been proposed based on the slot waveguides [22-25]. A compact PBS can be built incorporating the vertical slot waveguides [26]. However, the fabrication process for this PBS needs to etch the vertical slot in a nano-size region, which is not trivial to get the smooth interfaces. Instead of a vertical slot waveguide, a horizontal slot waveguide based PBS just needs to deposit different thicknesses for the vertical layers and then normally etch the waveguide [27]. A PBS has been reported to obtain an ER of > 20 dB by using two horizontal single-slot waveguides [28]. But, this PBS suffers from a long coupling-length of 65.87 μm and tight fabrication tolerance. Horizontal multiple-slotted waveguides have been reported to achieve a PBS with the cross-talk of -27.9 dB and -36.5 dB for the quasi-TE and quasi-TM modes, respectively [29].

Nevertheless, this structure also had an exceedingly long length of 238.0 μm and very tight fabrication tolerance.

In this paper, we design and optimize a fabrication-tolerant and compact PBS incorporating the horizontal triple-slot waveguides. Instead of multiple low-index layers inserted in the high-index layers for the conventional horizontal multiple-slot waveguide [21,29], we propose a novel triple-slot waveguide, in which two high-index nano-layers are embedded in three low-index silica-layers and this composite silica-waveguide is sandwiched by two outside silicon-layers. There are two motivations for this arrangement. First, with the increase in the thickness for the low-index layers, the field concentration is expected to slightly decrease, which can increase the coupling between two parallel waveguides. Consequently, the coupling length can be reduced and the fabrication tolerances also can be improved significantly. Second, simulation results show that the coupling length of the proposed PBS can be shortened by using a reduced thickness of the inner silicon nano-layers.

In this case, the modal characteristics for the isolated and composite waveguides are calculated by utilizing a rigorous **H**-field based full-vectorial finite element method (VFEM). Subsequently, the modal evolutions and fabrication tolerances for the proposed PBS are studied by utilizing the least squares boundary residual (LSBR) method. By careful design optimization, it is shown here that a fabrication-tolerant PBS with a compact length of 33 μm can be achieved using a novel horizontal triple-slot waveguides based structure. It can be noted that the length of our proposed PBS is only half and one-seventh length of the conventional horizontal single-slot waveguides [28] and multiple-slot waveguides [29] based PBSs, respectively. Besides that, simulations also show that, the fabrication tolerances can be improved substantially.

2. Theory

Since the cross-section of the proposed PBS has a multi-layer boundary, it is essential to accurately find the isolated mode and supermode profiles of the horizontal triple-slot waveguides. The VFEM based on the **H**-field can serve as a powerful method to calculate the effective indices and modal fields for the horizontal triple-slot waveguides based PBS [30,31]. This VFEM is one of the most rigorous methods to characterize the horizontal triple-slot waveguides as the **H** field is naturally continuous at the interfaces. Therefore, the modal characteristics for the composite horizontal-triple-slot waveguides are calculated by using the VFEM, which are subsequently used to calculate the coupling length for two polarizations. The full-vectorial variational formation as used in the VFEM can be given [30]:

$$\omega^2 = \frac{\iint \left[(\nabla \times \mathbf{H})^* \cdot \varepsilon^{-1} (\nabla \times \mathbf{H}) + p (\nabla \cdot \mathbf{H})^* (\nabla \cdot \mathbf{H}) \right] dxdy}{\int \mathbf{H}^* \cdot \mu \cdot \mathbf{H} dxdy} \quad (1)$$

where ω, ε and μ are the eigenvalue, permittivity and permeability, respectively. Here, p is a weighting factor for the penalty term, **H** is the full-vectorial magnetic field of the waveguide and * denotes the complex conjugate.

In this work, the modal evolutions and fabrication tolerances are accurately studied by utilizing a LSBR method for the horizontal triple-slot waveguides based PBS. By imposing the continuity of transverse Electric and Magnetic fields at the interface, the LSBR method can calculate the optical power for both the transmitted and reflected fields [32]. Combing with the VFEM, the LSBR method can accurately calculate the insertion loss, modal evolution, wavelength dependence and fabrication tolerances for the horizontal-triple-slot waveguide based PBS [33]. In this paper, the modal characteristics for the isolated and composite horizontal triple-slot waveguides are calculated based on the VFEM, in which the coupling length can be determined. Following that, the modal evolutions and fabrication tolerances are thoroughly studied by using the combination of the VFEM and LSBR method, respectively. The concept of the LSBR method is based on the

minimization of the error energy functional, J, to achieve a stationary solution, which enforces the continuity conditions for both the tangential E and H fields. The error energy functional, J, can be expressed as [31]

$$J = \int \left| E_t^I - E_t^{II} \right|^2 + \alpha \cdot Z_0^2 \left| H_t^I - H_t^{II} \right|^2 d\Omega \quad (2)$$

where E_t^I, H_t^I and E_t^{II}, H_t^{II} are the tangential electric and magnetic fields in sections I and II, respectively. α, Z_0 and Ω are the dimensionless weighting factor, free-space impedance and junction interface, respectively.

In this paper, the modal characteristics for the isolated and composite horizontal triple-slot waveguides are calculated based on the VFEM, in which the coupling length can be determined. Following that, the modal evolutions and fabrication tolerances are thoroughly studied by using a combination of the VFEM and LSBR method. The in-house VFEM and LSBR codes, developed and refined over three decades are used in this work.

3. Results

The proposed PBS consists of two parallel horizontal-triple-slot waveguides with a silica cladding is shown in Fig. 1. Compared to the conventional horizontal-multiple-layered slot waveguide [21], the proposed structure consists of two high-index nano-layers embedded in three low-index silica-layers and this composite silica-waveguide is sandwiched by two outside amorphous-silicon (a-Si) layers. With the increase in the thicknesses for the low-index layers, the field concentration is expected to decrease, which can substantially reduce the coupling length and can also improve the fabrication tolerances. The proposed PBS can be fabricated by using the conventional CMOS process described in [34], in which the propagation loss for the horizontal-triple-slot waveguide was measured to be 7.0 ± 0.20 dB/cm.
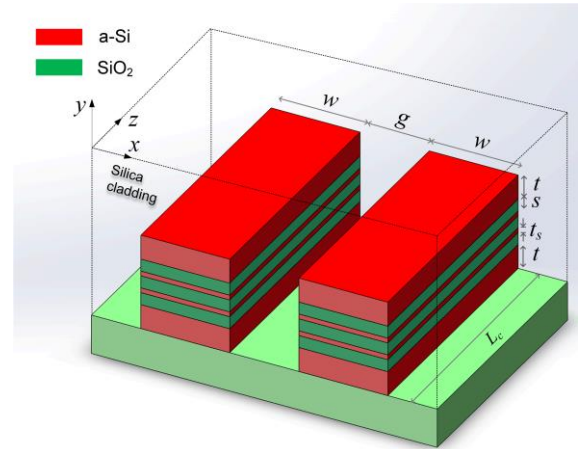

Fig. 1. Structure of the proposed PBS incorporating the horizontal triple-slot waveguides.

The thicknesses of the outside a-Si-layer, inner silica-layer and inner a-Si-layer are defined as t, s and t_s, respectively. Refractive indices of a-Si and SiO₂ are taken as 3.476 and 1.46, respectively at the operating wavelength of 1.55 μm. The separation between two horizontal-triple-slot waveguides is denoted by g. The width and device length for the horizontal triple-slot waveguide are denoted by w and L, respectively.

The normal electric field component E_y, for the quasi-TM mode of the horizontal triple-slot waveguide should undergo a large discontinuity as a result of the big index-difference between the a-Si and silica layers. In order to characterize the modal fields for the horizontal triple-slot waveguide, initially the parameters of w = 300 nm, t = 150 nm, t_s = 10 nm and s = 50 nm, are chosen. The field profiles for both the polarizations are shown in Fig. 2. It can be noted from Fig. 2(b) that for the quasi-TM mode, the normal E_y, component is strongly enhanced in the low-index silica-layers because of the large

discontinuity for the electric field at the a-Si-silica interfaces. Whereas for the quasi-TE mode, the dominant electric field E_x, component is mainly confined in the high-index a-Si layers, as shown in Fig. 2(a).
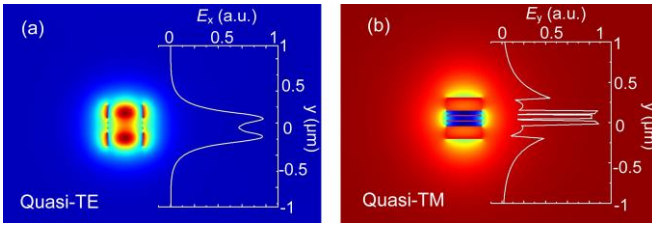

Fig. 2. Field profiles for (a) quasi-TE and (b) quasi-TM modes.

For the design of a DC based PBS, it is essential to study the modal characteristics of the supermodes for both the polarizations. Initially, identical thickness is chosen for the inner silica-layer, s and the inner a-Si-layer, t_s as a special case in between our proposed waveguide and the conventionally horizontal multiple-slot waveguide [21]. To study the modal fields and effective index for the supermode, the horizontal triple-slot waveguide with the parameters of $w = 400$ nm, $t = 60$ nm, $s = t_s = 20$ nm, is considered here. Variations of the effective indices of the supermodes as a function of the waveguide gap, g, are shown in Fig. 3. The even and odd supermodes for the quasi-TE mode are shown by two solid black and red lines, respectively. On the other hand, the even and odd supermodes for the quasi-TM mode are shown by two solid blue and pink lines, respectively. We can observe from Fig. 3 that the effective indices of the even supermodes for both the polarizations decrease as the waveguide gap increases, but for the odd supermodes increase with the increase in the gap. We can also observe that with sufficiently large gap, the effective indices for both supermodes converge to the isolated effective indices of two polarizations, respectively. It should be noted that the effective index of the quasi-TM mode is smaller than that of the quasi-TE mode due to the slight increase of the thickness for the low-index silica-layers. While the opposite results of the effective indices for two polarizations are shown in the conventional horizontal-multiple-slot waveguide [21], [29]. Moreover, the effective indices of the quasi-TE supermodes may converge more rapidly than those of the quasi-TM supermodes as a result of the normal E_y, component confined in the low-index regions. Therefore, a more compact PBS could be achieved by utilizing the proposed horizontal-triple-slot waveguides.
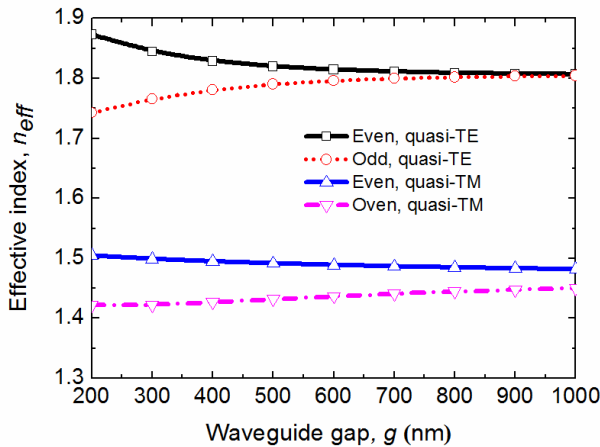

Fig. 3. Effective index, n_{eff}, for the supermodes as a function of the gap, g.

Coupling lengths for both the polarizations are obtained by using the formula as $L_c = \pi/(\beta_{even}-\beta_{odd})$, where β_{even} and β_{odd} are the propagation constants for the even and odd supermodes, respectively [33]. The concept of the proposed DC based PBS is to optimize a device which satisfies, $L = L_{TE} = 2L_{TM}$, where L_{TE} and L_{TM} are the coupling lengths for the quasi-TE and quasi-TM modes, respectively. First, the thicknesses of the inner silica-layer, s and inner a-Si-layers, t_s need to be appropriately chosen. A DC, consisting of two horizontal triple-slot

waveguides with $w = 400$ nm, $t = 150$ nm, $t_s = 20$ nm and $g = 300$ nm, are initially considered to analyze the influence of the thickness for the inner silica-layer.
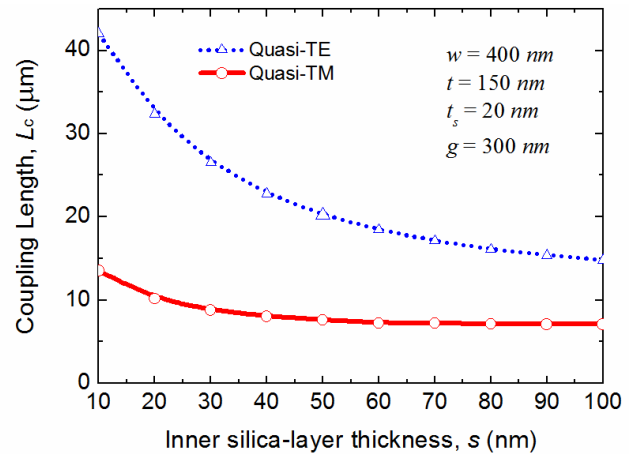

Fig. 4. The coupling lengths as a function of the inner silica thickness, s, for two polarizations.

Variations of the coupling lengths as a function of the inner silica thickness, s, are shown in Fig. 4 by the dotted blue and solid red lines for the quasi-TE and quasi-TM modes, respectively. We can observe that the coupling lengths for both the polarizations decrease with the increase in the thickness for the inner silica-layer. Therefore, a more compact PBS should be obtained by increasing the thickness of the inner silica-layer. However, a thicker slot-layer can cause the weaker confinement of the optical mode, and larger field at the dielectric interfaces will increase the propagation loss of the horizontal triple-slot waveguide [28]. In this case, the slot thickness, $s = 50$ nm, is chosen to balance the propagation loss and the coupling length.

Next, the horizontal-triple-slot waveguides with $w = 400$ nm, $t = 150$ nm, $s = 50$ nm and $g = 300$ nm, are considered to study the impact of the thickness of the inner a-Si-layers. Variations of the coupling lengths with the thickness of the inner a-Si-layers, t_s, for two polarizations are shown in Fig. 5. The coupling lengths for the quasi-TE and quasi-TM modes are shown by the dotted blue and solid red lines, respectively. We can observe from Fig. 5 that the coupling lengths for both the polarizations increase with the increase in the thickness, t_s. Considering the ease of fabrication, $t_s = 10$ nm, is chosen in this case.
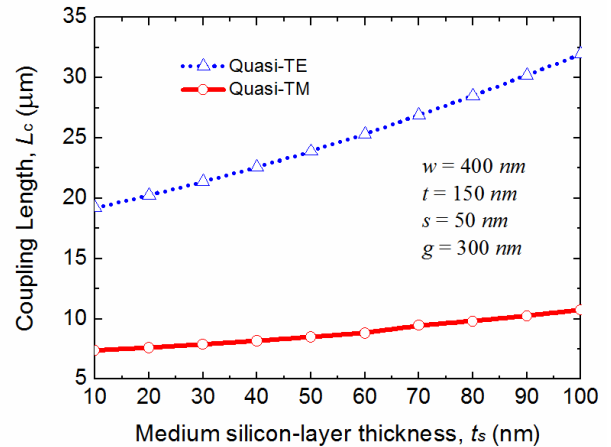

Fig. 5. Variations of coupling length with the inner a-Si thickness, t_s.

Next, ratios of the coupling length, L_{TE}/L_{TM}, as a function of the waveguide gap, g are calculated and shown in Fig. 6. In the calculation, the thicknesses of the inner silica-layer, s and inner a-Si-layers, t_s are chosen as 50 nm and 10 nm, respectively. The desired ratio, $L_{TE}/L_{TM} = 2$ is shown by a horizontal solid-black line. It can be observed from Fig. 6 that ratios of the coupling lengths, L_{TE}/L_{TM}, increase as the gap, g, increases. There are several points, where this unique ratio $L_{TE}/L_{TM} = 2$

can be obtained. As examples, these are, for $w = 400$ nm and $t = 200$ nm with $g = 124.5$ nm, for $w = 400$ nm and $t = 150$ nm with $g = 208$ nm, for $w = 400$ nm and $t = 100$ nm with $g = 419$ nm, for $w = 300$ nm and $t = 200$ nm with $g = 621$ nm, for $w = 300$ nm and $t = 150$ nm with $g = 654$ nm and for $w = 300$ nm and $t = 100$ nm with $g = 868.5$ nm. In these cases, the devices lengths, $L = L_{TE} = 2L_{TM}$ are 7.5 μm, 10.3 μm, 20 μm, 48 μm, 33 μm and 38 μm, respectively. Although a shorter PBS length can be achieved with a smaller waveguide gap, however, the cross-talk can be higher [28]. Considering the coupling length and the cross-talk, the device length, $L = L_{TE} = 2L_{TM} = 33$ μm and waveguide gap, $g = 654$ nm are chosen for the horizontal triple-slot waveguide with $w = 300$ nm and $t = 150$ nm for further evaluations.
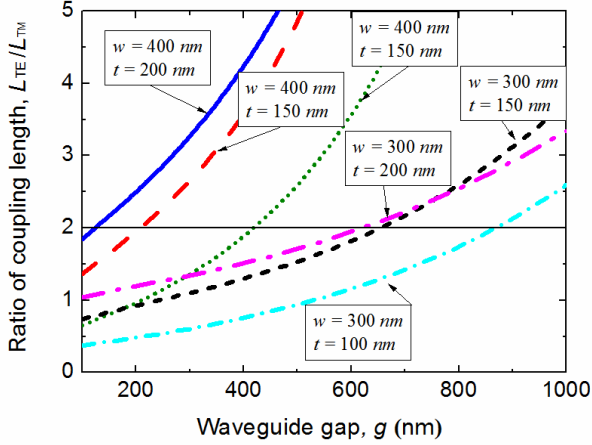

Fig. 6. The ratios of the coupling length, L_{TE}/L_{TM} as a function of the waveguide gap.
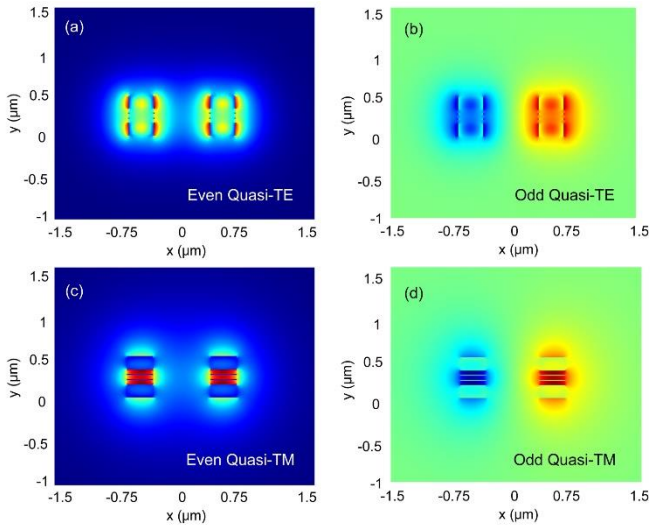

Fig. 7. Supermode field profiles, (a) E_x field of even-like quasi-TE, (b) E_x of odd-like quasi-TE, (c) E_y of even-like quasi-TM and (d) E_y of odd-like quasi-TM modes.

The supermode field profiles for $L = L_{TE} = 2L_{TM}$ are calculated by using the VFEM and are shown in Fig. 7. We can observe that the E_y fields for the quasi-TM supermodes are mostly confined in the low-index silica-layers, while the E_x fields for the quasi-TE supermodes are mostly confined in the high-index a-Si-layers. The evolutions of the optical fields along z direction are studied by using the LSBR method and shown in Figs. 8 (a) and (b) for the quasi-TE and quasi-TM modes, respectively. We can observe that a complete power-transfer from the bar-port to the cross-port can be achieved for the quasi-TE mode. Meanwhile, the optical power for the quasi-TM mode is firstly transferred to the cross-port and then brought back totally to the bar-port. The numerically simulated results show that the insertion losses are 0.07 dB and 0.1 dB for the quasi-TE and quasi-TM modes,

respectively. Therefore, an efficient PBS can be achieved incorporating the horizontal triple-slot waveguides with the parameters of $w = 300$ nm, $g = 654$ nm, $t = 150$ nm, $s = 50$ nm, $t_s = 10$ nm and $L = L_{TE} = 2L_{TM} = 33$ μm.
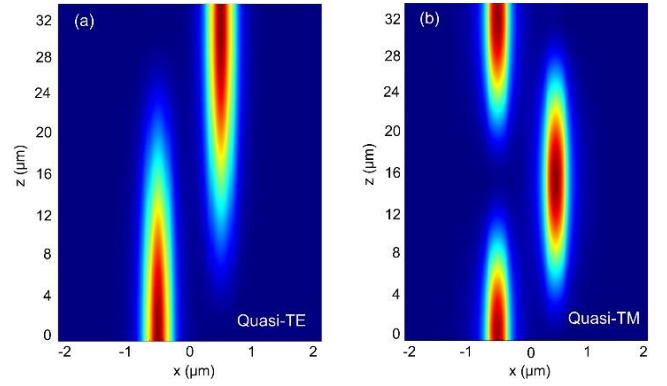

Fig. 8. Optical fields along z direction for (a) quasi-TE and (b) quasi-TM modes, respectively.

The wavelength dependence on the bar- and cross-port outputs for both the polarizations are calculated by utilizing the LSBR method and shown in Fig. 9. We can observe that the maximum polarization extinction ratios (PERs) can be obtained as -21.8 dB and -20.3 dB for the quasi-TE and quasi-TM modes, respectively, at the 1.55 μm wavelength. We also can observe that the 1 dB bandwidth is almost 100 nm for both the polarizations, which is better than that of the conventional horizontal-single-slot waveguide based PBS [28] reported earlier. Our design, the cross-talks are 12.66 dB and 19.15 dB at $λ = 1540$ nm and these are 12.8 dB and 19.04 dB at $λ = 1560$ nm for the quasi-TE and quasi-TM modes, respectively. We can observe that the transmittance for the quasi-TM mode is less sensitive to the wavelength variations, which is due to the stronger coupling for the quasi-TM mode. Therefore, weakly confined quasi-TM mode is more stable with the wavelength variation than that for the quasi-TE mode.
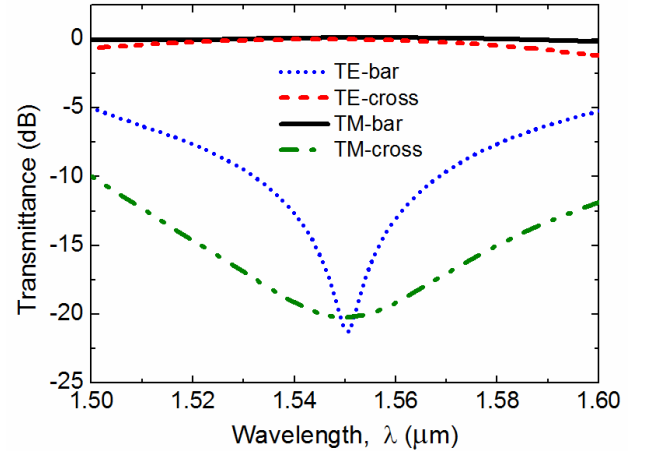

Fig. 9. Variations of the transmittance with the wavelength for two polarizations.

A fabrication-tolerant PBS is of great importance to guarantee the performance in practice, since both the conventional horizontal-single-slot and multiple-slot waveguides based PBSs suffer from the limitation of the tight fabrication tolerance [28,29]. In this case, a fabrication-tolerant PBS can be achieved based on the horizontal-triple-slot waveguides and the fabrication tolerances are studied by using the LSBR method in detail. Variations of the transmittance with the device length, L for both the polarizations are shown in Fig. 10. When $L = L_{TE} = 2L_{TM} = 33$ μm, the PERs are -21.8 dB and -20.3 dB for the quasi-TE and quasi-TM modes, respectively. The cross-talks are 19.62 dB and 17.8 dB when $L = 32$ μm and these are 19.61 dB and 17.8

dB when L = 34 μm for the quasi-TE and quasi-TM modes, respectively. We can also observe that the transmittance deteriorates by 1 dB and 2.5 dB for the device-length variation of ±5 μm for the quasi-TE and quasi-TM modes, respectively. As stated earlier, the coupling length for the quasi-TM mode, L_{TM}, was half of the L_{TE}. So the phase error for a given ΔL is double for the quasi-TM mode.
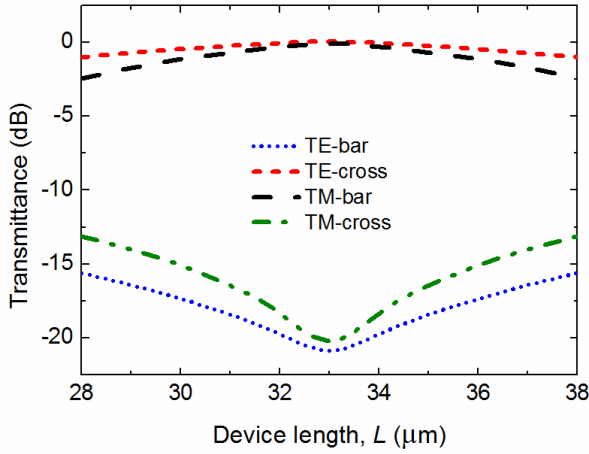

Fig. 10. The transmittance as a function of the device length for two polarizations.

The transmittance as a function of the waveguide width, w for both the polarizations are shown in Fig. 11. We can observe that, even when width is changed by ± 10 nm, the resulting transmission deterioration was only 1 dB for both the quasi-TE and quasi-TM modes, while the tolerance to the width is very critical for the quasi-TE mode of the horizontal single-slot waveguide based PBS [28]. We can also observe that the cross-talks are 11.93 dB and 18.67 dB when w = 295 μm and these are 12.21 dB and 18.67 dB when w = 305 μm for the quasi-TE and quasi-TM modes, respectively.
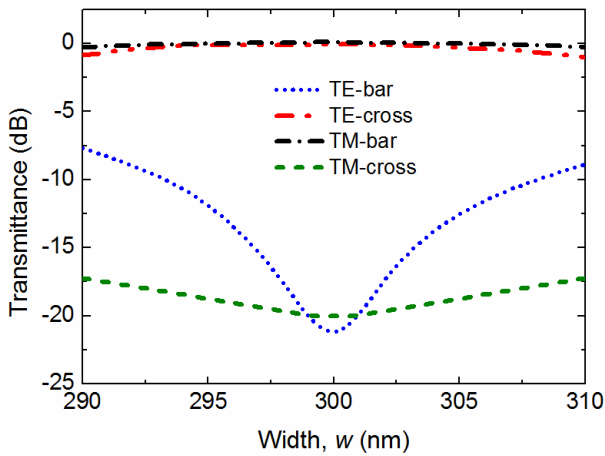

Fig. 11. The transmittance as a function of the waveguide width for two polarizations.

Next, the transmittance as a function of the waveguide gap, g for both the polarizations are calculated and shown in Fig. 12. We can observe that, even when waveguide-gap is changed by ± 10 nm, the resulting transmission deterioration was less than 0.04 dB for both the polarizations, while the variation of the transmittance is very sensitive to the waveguide gap for two polarizations of the conventional horizontal-multiple-slot waveguide based PBS [29]. It also can be observed that a low cross-talk (-15 dB) over a wider waveguide-gap change, Δg of 20 nm can be easily achieved.
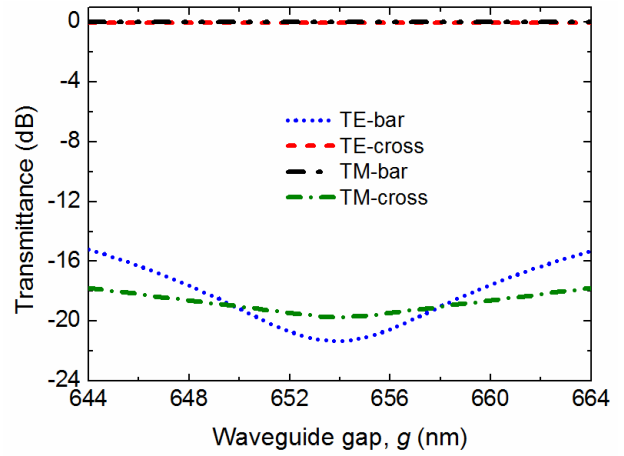

Fig. 12. The transmittance as a function of the waveguide gap for two polarizations.

Finally, tolerances to the thickness variation of the outside a-Si-layers, t, inner a-Si-layers, t_s, and inner silica-layers, s are studied. The transmittance as a function of the outside a-Si-layer thickness, t for two polarizations are shown in Fig. 13. We can observe that even when thickness is changed by ± 10 nm, the resulting transmission deterioration was only 1 dB for both the quasi-TE and quasi-TM modes. It can be observed that the cross-talks are 15.57 dB and 17.36 dB when t = 145 μm and these are 13.78 dB and 17.32 dB when t = 155 μm for the quasi-TE and quasi-TM modes, respectively. We can also observe that the tolerance is less critical for the quasi-TM mode than that for the quasi-TE mode. The reason can be explained as the quasi-TE mode mainly confined in the a-Si layers, while the quasi-TM mode is mostly confined in the low-index silica-layers. Therefore, the influence of the t, on the transmittance is much smaller for the quasi-TM mode than that for the quasi-TE mode.
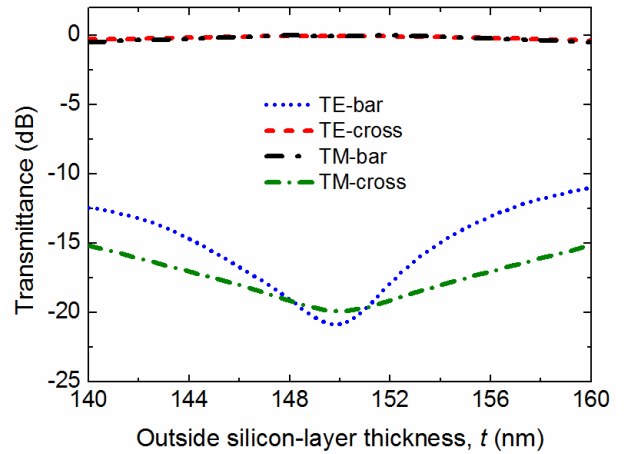

Fig. 13. The transmittance as a function of the outside a-Si-layer thickness for two polarizations.

Variations of the transmittance with the inner a-Si-layers thickness, t_s for both the polarizations are shown in Fig. 14. It can be observed that when the inner a-Si-layers thickness is changed from t_s = 5 nm to 20 nm, the resulting transmission deterioration was less than 0.15 dB for both the quasi-TE and quasi-TM modes. Variations of the transmittance with the inner silica-layer thickness, s are shown in Fig. 15. We note that the inner silica-layer thickness is changed from s = 40 nm to 60 nm, the resulting transmission deterioration was less than 0.2 dB for both the polarizations. A low cross-talk (-15 dB) can be retained over a wider variation of thickness by ± 10 nm. It also can be observed from Figs. 14 and 15 that the quasi-TM mode is more dependent on the thicknesses of the inner silica-layer and inner a-Si-layers, compared to the quasi-TE mode. The reason for this is that the

quasi-TE mode is more confined in the outside a-Si-layers than in the central areas, while the quasi-TM mode is strongly confined in the low-index silica-layers.
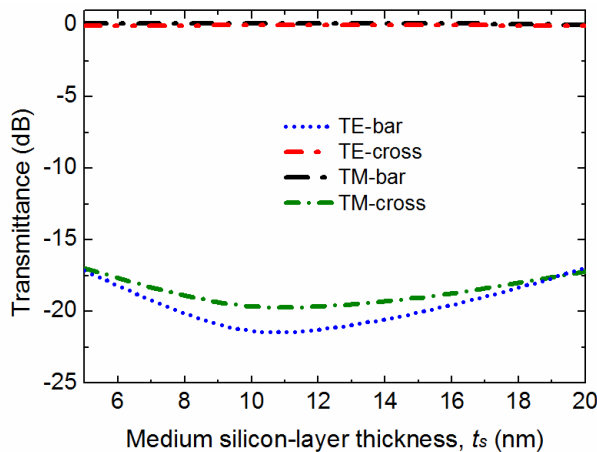

Fig. 14. The transmittance as a function of the inner a-Si-layers thickness for two polarizations.
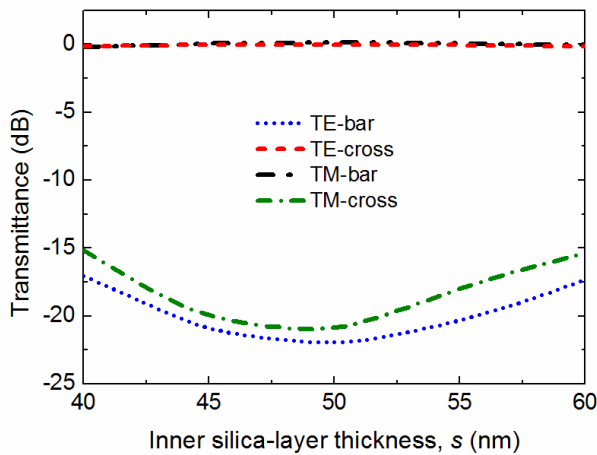

Fig. 15. The transmittance as a function of the inner silica-layer thickness for two polarizations.
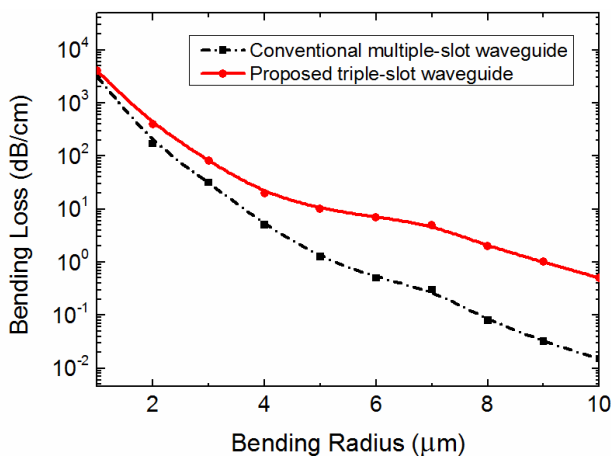

Fig. 16. Variations of the bending loss for conventional horizontal multiple-slot waveguide and proposed waveguide with the bending radius.

The bending characteristics are very important for the actually photonic integrated device. Variations of the bending loss for the conventional horizontal multiple-slot waveguide and proposed waveguide with the bending radius are calculated and were reported in Fig. 16. The conventional horizontal multiple-slot waveguide is cited from Fig. 9 in Reference [21]. The proposed triple-slot waveguide has

the following device parameters, w = 300 nm, t = 150 nm, s = 50 nm, and t_s = 10 nm. It can be stated that the proposed horizontal triple-slot waveguide exhibits slightly higher bending loss as the conventional horizontal multiple-slot waveguide. However, for a design incorporating 5 μm bending radius, a 90 degree bend (length of the bent section is less than 8 μm) total loss would be less than 0.01 dB.

4. Conclusions

In conclusion, a fabrication-tolerant and compact PBS is proposed and optimized incorporating the horizontal triple-slot waveguides, which consists of two high-index nano-layers embedded in three low-index silica-layers and this composite silica-waveguide is sandwiched by two outside a-Si-layers. The proposed PBS design has been optimized by using an efficient algorithm, combining the **H**-field based VFEM and the LSBR method. The modal field profiles for the vector modes and supermodes have been calculated by using the VFEM. Following that, the modal evolutions and fabrication tolerances have been studied by using the LSBR method. A fabrication-tolerant PBS with a compact length of 33 μm has been obtained based on the horizontal triple-slot waveguides. The PERs reach -21.8 dB and -20.3 dB for the quasi-TE and quasi-TM modes, respectively at λ = 1.55 μm. The 1dB bandwidth of 100 nm wavelength variation can be achieved for both the polarizations. The numerically simulated results have also shown that the proposed PBS is stable with the variation of the device parameters. For device length, L variation of ±5 μm, the transmittance deteriorates by 1 dB and 2.5 dB for the quasi-TE and quasi-TM modes, respectively. For the variation of ± 10 nm for w, g and t, the resulting transmission deterioration was only 1 dB for both the polarizations. For the variation from t_s = 5 nm to 20 nm, the resulting transmission deterioration is less than 0.15 dB for both the polarizations. For the variation from s = 40 nm to 60 nm, the resulting transmission deterioration is less than 0.2 dB for both the polarizations. The presented PBS exhibits better performance compared to the previously reported designs, and can be considered for the polarization control and manipulation in the polarization diversity scheme.

References

1. M. Asghari and A. V. Krishnamoorthy, "Silicon photonics: Energy-efficient communication," Nature Photon. **5**, 268–270 (2011).
2. B. Jalali and S. Fathpour, "Silicon photonics," J. Lightwave Technol. **24**, 4600–4615 (2006).
3. D. Dai, J. Bauters, and J. E. Bowers, "Passive technologies for future large-scale photonic integrated circuits on silicon: polarization handling, light non-reciprocity and loss reduction," Light: Sci. Appl. **1**, 1–12 (2012).
4. J. T. Kim, "CMOS-compatible polarization splitter for 3-D silicon photonic integrated circuits," J. Lightwave Technol. **32**, 2123–2127 (2014).
5. S. Soudi and B. M. A. Rahman, "Design of compact polarization rotator using simple silicon nanowires," Appl. Opt. **53**, 8071–8077 (2014).
6. S. Soudi and B. M. A. Rahman, "Design of a compact polarization splitter by using identical coupled silicon nanowires," J. Lightwave Technol. **34**, 4169–4178 (2016).
7. D. Dai, H. Wu, and W. Zhang, "Utilization of field enhancement in plasmonic waveguides for subwavelength light-guiding, polarization handling, heating, and optical sensing," Materials, **8**, 6772–6791 (2015).
8. T. Yamazaki, H. Aono, J. Yamauchi, and H. Nakano, "Coupled waveguide polarization splitter with slightly different core widths," J. Lightwave Technol. **26**, 3528–53533 (2008).
9. B. Shen, P. Wang, R. Polson, and R. Menon, "An integrated-nanophotonics polarization beam splitter with 2.4 × 2.4 μm2 footprint," Nature Photon. 9, 378–382 (2015).

10. D. Dai, "Silicon polarization beam splitter based on an asymmetrical evanescent coupling system with three optical waveguides," J. Lightwave Technol. 30, 3281–3287 (2012).

11. Z. Wang, L. Shi, X. Xu, J. Zhang, J. Zhang, and X. Zhang, "Optical nonreciprocity with large bandwidth in asymmetric hybrid slot waveguide coupler," Opt. Express, **23**, 3690–3698 (2015).

12. K. Chang and C. Huang, "Ultrashort broadband polarization beam splitter based on a combined hybrid plasmonic waveguide," Sci. Rep. **6**, 9609 (2016).

13. H. Fukuda, K. Yamada, T. Tsuchizawa , T. Watanabe , H. Shinojima, and S. Itabashi, "Ultrasmall polarization splitter based on silicon wire waveguides," Opt. Express, **14**, 12401–12408 (2006).

14. D. Dai, Z. Wang, and J. E. Bowers, "Ultra-short broad-band polarization beam splitter based on an asymmetrical directional coupler," Opt. Lett. **36**, 2590–2592 (2011).

15. I. Kiyat, A. Aydinli, and N. Dagli, "A compact silicon-on-insulator polarization splitter," IEEE Photon. Technol. Lett. **17**, 100–102 (2005).

16. C. Hsu, T. Chang, J. Chen, and Y. Cheng, "8.13 μm in length and CMOS compatible polarization beam splitter based on an asymmetrical directional coupler," Appl. Opt. **55**, 3313–3318 (2016).

17. L. Han, S. Liang, H. Zhu, C. Zhang, and W. Wang, "A high extinction ratio polarization beam splitter with MMI couplers on InP substrate," IEEE Photon. Technol. Lett., vol. 27, no. 7, pp. 782–785 (2015).

18. H. Qiu, "Compact polarization splitter based on silicon grating-assisted couplers," Opt. Lett. **40**, 1885–1887 (2015).

19. V. R. Almeida, Q. Xu, C. A. Barrios, and M. Lipson, "Guiding and confining light in void nanostructure," Opt. Lett. **29**, 1209–1211 (2004).

20. M. Lipson, "Guiding, modulating, and emitting light on silicon-challenges and opportunities," J. Lightwave Technol. **23**, 4222-4238 (2005).

21. N. Feng, J. Michel, and L. C. Kimerling, "Optical field concentration in low-index waveguides," IEEE J. Quantum Electron. **42**, 883–888 (2006).

22. J. V. Galan, P. Sanchis, J. Garcia, J. Blasco, A. Martinez, and J. Martí , "Study of asymmetric silicon cross-slot waveguides for polarization diversity schemes," Appl. Opt. 48, 2693-2696 (2009).

23. H. Zhang, Y. Huang, S. Das, C. Li, M. Yu, P. G. Lo, M. Hong, and J. Thong "Polarization splitter using horizontal slot waveguide," Opt. Express, 21, 3363–3369 (2013).

24. S. Lin, J. Hu, and K. B. Crozier, "Ultra-compact, broadband slot waveguide polarization splitter," Appl. Phys. Lett. **98**, 151101 (2011).

25. Y. Ma, M. Sung, and D. Huang, "Controlling the polarization dependence of dual-channel directional couplers formed by silicon-on-insulator slot waveguides," Appl. Opt. **49**, 6979–6985 (2010).

26. H. Zhang, J. Zhang, S. Chen, J. Song, J. S. Kee, M. Yu, and G. Q. Lo, "CMOS-compatible fabrication of silicon-based sub-100-nm slot waveguide with efficient channel-slot coupler," IEEE Photon. Technol. Lett. **24**, 10–12 (2012).

27. Y. Yue, L. Zhang, J. Yang, R. G. Beausoleil, and A. E. Willner, "Silicon-on-insulator polarization splitter using two horizontally slotted waveguides," Opt. Lett. **35**, 1364–1366 (2010).

28. N. Cheng, Y. Ma, P. Fu, C. Chin, and D. Huang, "Horizontal slot waveguides for polarization branching control," Appl. Opt. **54**, 436–443 (2015).

29. J. Xiao, X. Liu, and X. Sun, "Design of a compact polarization splitter in horizontal multiple-slotted waveguide structures," Jpn. J. Appl. Phys. **47**, 3748–3754 (2008).

30. B. M. A. Rahman and J. B. Davies, "Finite-element solution of integrated optical waveguides," J. Lightwave Technol. **2**, 682–688 (1984).

31. A. Barh, B. M. A. Rahman, R. K. Varshney, and B. P. Pal, "Design and performance study of a compact SOI polarization rotator at 1.55 μm," J. Lightwave Technol. **31**, 3687–3693 (2013).

32. B. M. A. Rahman and J. B. Davies, "Analysis of optical waveguide discontinuities," J. Lightwave Technol. **6**, 52–57 (1988).

33. W. Jiang, N. Kohli, X. Sun, and B. M. A. Rahman, "Multi-poly-silicon-layer based spot-size converter for efficient coupling between silicon waveguide and standard single-mode fiber," IEEE Photonics J. **8**, 6600612 (2016).

34. R. Sun, P. Dong, N. Feng, C. Y. Hong, J. Michel, M. Lipson, and L. Kimerling, "Horizontal single and multiple slot waveguides: optical transmission at λ= 1550 nm," Opt. Express, **15**, 17967-17972 (2007).